e-ISSN: 2550-164X

Available online at
https://jmeche.uitm.edu.my/

Journal of Mechanical Engineering 23(1) 2026, 39 – 62.

Journal of Mechanical Engineering

Analysis of Uniaxial Stress State of an Infinite Sheet with Complex Geometry: Impact of Elliptical Holes and Linear Cracks on Structural Stability

Etimad Eyvazov[1*], Gasım Abdullayev[2]

[1]*Department of Mechanics, Azerbaijan University of Architecture and Construction, Baku, Azerbaijan*
[2]*Department of Transport and Logistics, Azerbaijan University of Architecture and Construction, Baku, Azerbaijan*

ARTICLE INFO

Article history:
Received 14 March 2025
Revised 21 July 2025
Accepted 20 August 2025
Online first
Published 15 January 2026

Keywords:
Analytical functions
Elliptical holes
Intensity factor
Conformal mapping functions
Stress components

DOI:
10.24191/jmeche.v23i1.5703

ABSTRACT

In engineering design, structural defects such as cracks can lead to catastrophic failures in machines and equipment. This study investigates the uniaxial stress state of an infinite sheet weakened by two elliptical holes with linear cracks. Due to the complexity of the geometric configuration and the absence of known conformal mapping functions for such regions, this problem has not been addressed in previous research. We solve a plane elasticity problem for a complex geometric configuration featuring two elliptical holes with linear cuts using the theory of complex variables and conformal mapping functions. The solution involves solving a system of linear algebraic equations derived from the theory of complex variables and Kolosov-Muskhelishvili potentials. By expanding the functions $\varphi(z)$ and $\psi(z)$ into series, we obtain an analytical solution and provide numerical examples to illustrate key theoretical aspects. The coefficients of the analytical functions are determined, and well-known elasticity theory formulas are applied to compute stress components at characteristic points. This research presents a novel approach to solving this specific problem, as conformal mapping functions for such complex configurations have not been previously established.

INTRODUCTION

Conformal mapping has numerous applications in solving practical problems in the field of mechanical engineering with the use of new functions of the theory of complex variables for different areas having a complex geometric configuration. In this article, the problem is solved for the first time using new functions of the theory of functions of a complex variable. The article deals with the stress-strain state of an infinite isotropic sheet, weakened by two symmetrical holes of complex configuration and with linear cracks. The presented product has a three-connected area, bounded from the inside by two elliptical holes with semi-

[1*] Corresponding author. *E-mail address*: eyvazovetimad480@gmail.com
https://doi.org/10.24191/jmeche.v23i1.5703

axes a and b. The outlines surrounding these ellipses are designated L_1 and L_2, respectively. Outside, the square or endless strip is bounded by two parallel lines. The centres of the elliptical holes are located on the real axis Ox, and the distance between these centres is $2l$. The origin of the O coordinate system is in the middle of the centres O_1 and O_2. Coordinates of the ends of linear cracks: (l_1±e) for the hole on the right and (l_1±e) for the hole on the left. Straight cutouts (cracks) lie on the Ox axis. The holes, i.e., ellipses from the inside, are not subject to external stress. A tensile force with intensity p is applied to the infinite sheet along the ordinate. In the study of the uniaxial stress state of an infinite sheet with complex geometry, weakened by elliptical holes and linear cracks, it is important to focus on the presence of these elliptical holes and linear cracks in the sheet's geometry, which leads to significant stress concentration in these areas. This can result in undesirable local increases in stress, potentially causing material failure or deformation.

The problem studied in this area covers the analysis of an infinite strip with a complex geometric shape, which looks like an ellipse. Mukhopadhyay & Mishra (2024) determined that an ellipse has two semi-axes: major and minor. The researcher also determined how these semi-axes affect the behaviour and characteristics of the elliptic region. As part of the study, Guo et al. (2024a) determined that two symmetric cracks located on the real axes of the ellipse are also accounted for. These cracks have a significant impact on the behaviour and characteristics of the area under investigation, which requires special attention during the analysis. Issues that require further study include the development of conformal mapping. Such a mapping is important for simplifying complex geometric shapes and analysing their properties. Another important task is to analyse the conformal mapping function. These functions simplify the problem by converting the complex configuration of a cracked ellipse into a simpler form, which facilitates further analysis and calculations.

Li et al. (2024) and Wang et al. (2024) analysed and developed strategies to preserve the geometric characteristics of the area. They determined the shape of this area, which in this case is an ellipse with cracks, which is key to accurate research and analysis. Wu et al. (2024) analysed and established the correlation between the number of selected conformal mappings. The author identified how these mappings could simplify the area, transforming it into a more analytically friendly form. Issues that require further study include assessing the impact of transforming a problem into a simplified form. After converting the area to a more convenient form for analysis, it is necessary to determine how this will affect the application of standard methods to solve the problem. Further research is needed to verify the stability of the results. After the results obtained for the simplified domain are transferred back to the original form, it is necessary to check their accuracy and stability to ensure the final solution. Another topical issue in this area is that the second problem uses analytical regular functions from the theory of complex functions to solve a specific problem. This can be used for specialised mathematical methods that simplify and accurately solve the problem, which can be substantial for analysing complex systems or geometric configurations.

Cao et al. (2024) presented a methodology for determining optimal application rates using the theory of complex variable functions. This theory studies functions that are analytical (or regular) on the complex plane, which was used to develop accurate and efficient methods for solving problems. Zhao et al. (2024) and Lawlor et al. (2024) analysed analytical functions, which are functions that have a derivative at every point in their domain of definition and are continuous. They showed that the use of such functions can simplify the solution of problems involving complex geometric areas or conditions that are difficult to solve directly. The effectiveness of different formulas for solving the problem needs to be further studied. For this purpose, certain analytical functions are selected that best meet the conditions of the problem and help to optimally solve the problem.

Research into the development of hardening technologies may involve the selection of functions with specific properties, such as unit functions, simple polynomials, fractional rational functions, or other specialised functions. This can be used to adapt the methods to the specific conditions and requirements of

https://doi.org/10.24191/jmeche.v23i1.5703

the task to achieve the best results. The authors' goal is to study the stress-strain state of an endless strip with two elliptical holes and two symmetric cracks.

MATERIALS AND METHODS

This paper presents the essential equations for calculating the stresses at critical locations within the cross-sections of the plate. The system of linear algebraic equations was solved by representing the functions $\varphi(z)$ and $\psi(z)$ as series expansions. During the study, an analytical solution was obtained, and numerical examples were given to illustrate important aspects of the theory. By solving these linear algebraic equations, the coefficients of the analytical function were found, and the well-known formulas of the theory of elasticity were used to determine the stress components, and the stress components were also found at the characteristic points of the sections.

A qualitative analysis of stresses and deformations was conducted, and classifications were created, which allowed the identification and systematisation of the main factors affecting the stability of structures with complex geometry, particularly the presence of elliptical holes and linear cracks, leading to stress concentration and potential material failure. This enabled the development of targeted methods for effective protection and restoration of structures in the design of engineering tasks, where constructors often encounter various defects in structures, particularly cracks. The primary focus was on investigating and classifying the threats associated with the use of various strengthening technologies and methods within the study. The study included a comparative analysis and critical review of various technologies applied to solve a plane problem in elasticity theory with a complex geometric configuration, weakened by two elliptical holes with linear cuts. The effectiveness was evaluated by solving the problem, which was addressed through a system of linear algebraic equations using the theory of complex variables and Kolosov-Muskhelishvili potentials (Table 1).

Table 1. Symbol definitions

Category	Symbol	Description
Geometric Parameters	z	Complex coordinate in the physical plane
Geometric Parameters	ξ_1, ξ_2	Complex coordinates in the mapped plane (unit circles)
Geometric Parameters	L_1, L_2	Contours of the right and left elliptical holes, respectively
Geometric Parameters	l	Half-distance between hole centres
Geometric Parameters	a_1, b_1	Semi-major and semi-minor axes of the elliptical holes
Geometric Parameters	A_1, A_2	Mapping parameters, where $A_1 = A_2 = (a_1 + b_1)/2$
Complex Functions	$\varphi(z)$	Primary complex potential function
Complex Functions	$\psi(z)$	Secondary complex potential function
Complex Functions	$\chi(z)$	Modified potential function, defined as $\chi(z) = \psi(z) + z \cdot \varphi'(z)$
Complex Functions	$f(t,\bar{t})$	Boundary condition function on contours L_1 and L_2
Stress Components	σ_x, σ_y	Normal stress components in x and y directions
Stress Components	τ_{xy}	Shear stress component
Stress Components	σ_x^0, σ_y^0, τ_{xy}^0	Applied stress components at infinity
Stress Components	p, q	Applied forces in different directions
Series Coefficients	a_k, b_k	Unknown coefficients in the series expansions
Series Coefficients	Π_n, E_n, L_n	Coefficients in the conformal mapping functions

https://doi.org/10.24191/jmeche.v23i1.5703

The key parameters of the study were determined, including the geometric characteristics of the plate, the size of the elliptical holes, and the location and length of the linear cracks. The load conditions and boundary conditions for the plate were also established, which were used to accurately formulate the problem and ensure the correctness of further analysis. The conditions established account for both static and dynamic loads, which can be used to assess the real impact of defects on structural stability under conditions close to operational ones. The structural stability was assessed, and the stability of the structure was analysed, addressing the stress distribution obtained at the previous stage. The analysis identified potential areas of cracking or defects and assessed the risks of further expansion. The structure was tested for strength and stability to determine whether it meets the established safety requirements. Additionally, an analysis was carried out to assess the impact of parameter variations on the overall stability of the structure, which allows for a more complete picture of its changes under different loading conditions.

The first task was to consider an infinite strip with a complex configuration in the form of an ellipse with large and small semi-axes, as well as two symmetric cracks located on the real axes. For this purpose, the conformal mapping functions were found. The second task was to solve the problem using analytical regular functions of the theory of complex variables. Next, these contours were transformed into unit circles. After complex mathematical calculations, the problem was reduced to a system of two linear algebraic equations. The first few terms (coefficients) of these equations are then stored. To determine the normal and tangential stresses, we used special formulas from the plane problem of elasticity theory and calculated the stress components at certain points (Fig 1).

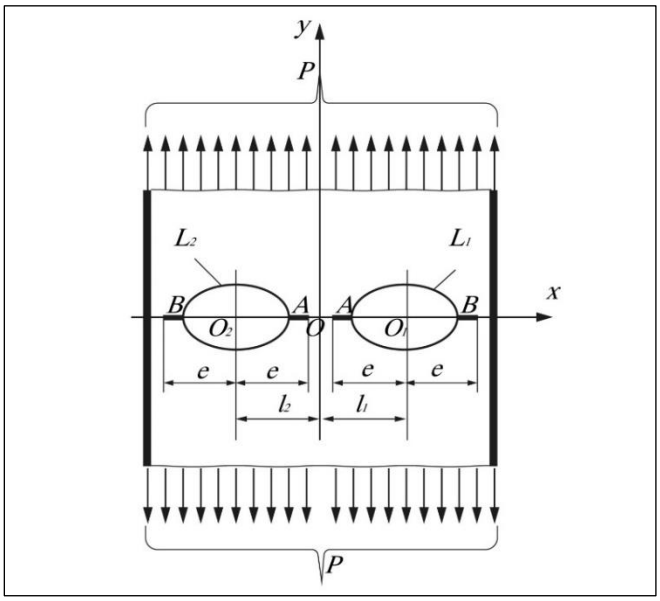

Fig. 1. Stress-strain state of infinite isotropic sheet weakened by two elliptical holes with linear cracks.

The problem begins with establishing the boundary conditions that must be satisfied on the hole contours. As is known, the solution to such problems is accomplished by finding complex potentials $\varphi(z)$ and $x(z)$ as boundary conditions, expressed in Equation 1:

$$\varphi(t) + (t - \overline{t}) \cdot \overline{\varphi'(t)} + \overline{\chi(t)} = f(t, \overline{t}) \tag{1}$$

https://doi.org/10.24191/jmeche.v23i1.5703

These boundary conditions differ slightly from the first boundary conditions shown in Equation 2:

$$\varphi(t) + t.\overline{\varphi'(t)} + \psi(t) = f\left(t, \overline{t}\right) \tag{2}$$

This differs from the standard first boundary condition by introducing the modified function $\chi(z)$. To simplify the mathematical treatment, the modified potential function is introduced in Equation 3:

$$\chi(z) = \psi(z) + z\varphi'(z) \tag{3}$$

This substitution transforms the boundary condition into a more convenient form for analysis. By applying the conjugate expression of *χ(z)* and substituting it into Equation 2, the boundary conditions can be transformed into the form of Equation 1. In Equation 1, *t* represents the affix of points of the contours L_1 and L_2. It should be indicated that the function $f\left(t, \overline{t}\right)$ is defined as follows in Equation 4:

$$f\left(t, \overline{t}\right) = -p\frac{1}{2}\left(\overline{t} + t\right) \pm C \tag{4}$$

If the forces *p* and *q* are applied to the sheet in both directions, then the expression can be written for $f\left(t, \overline{t}\right)$ as follows Equation 5:

$$f\left(t, \overline{t}\right) = \frac{q-p}{2}.\overline{t} - \frac{q+p}{2}.t \pm C \tag{5}$$

In this case, σ_x^0, σ_y^0 and τ_{xy}^0 values are as below for solid sheets: $\sigma_x^0 = q;\ \sigma_y^0 = p;\ \tau_{xy}^0 = 0$. And the constant *C* is negligible since it does not affect the stress state of the sheet. The stress state of the sheet during observation is determined by using Equation 6:

$$\begin{aligned}\sigma_x = \sigma_y = \sigma_x^0 + \sigma_y^0 + 4\,Re[\varphi'(z)]\,, \sigma_x - \sigma_y + 2i\tau_{xy} \\ = \sigma_y^0 - \sigma_x^0 + 2i\tau_{xy}^0 + 2[(\overline{z} - z)\varphi''(z) - \varphi'(z) + \chi'(z)]\end{aligned} \tag{6}$$

where, the stress compony σ_x^0, σ_y^0 and τ_{xy}^0 τ_{xy}^0, σ_x^0, σ_y^0 and τ_{xy}^0 belong to a solid sheet. And the stress components are as below for the problem in this case, Equation 7:

$$\sigma_x^0 = 0, \sigma_y^0 = 0, \tau_{xy}^0 = 0 \tag{7}$$

The function $\varphi(z)$ and *χ(z)* can be determined as follow Equation 8:

$$\varphi_1(z) = \varphi_1(z) + \varphi_2(z); \chi(z) = \chi_1(z) + \chi_2(z) \tag{8}$$

where, the functions $\varphi_1(z)$ and $\chi_1(z)$ are holomorphic functions out of hole L_1 and the functions $\varphi_2(z)$ and $\chi_2(z)$ are holomorphic functions out of hole L_2. The functions can be written as follows, since those functions are missing at infinite, Equation 9:

$$\varphi_1(z) = \sum_{k=1}^{\infty} a_k\,.\,\xi_1^{-k}, \varphi_2(z) = \sum_{k=1}^{\infty} a_k^*\,\xi_2^{-k} \tag{9}$$

https://doi.org/10.24191/jmeche.v23i1.5703

$$\chi_1(z) = \sum_{k=1}^{\infty} b_k . \xi_1^{-k}, \chi_2(z) = \sum_{k=1}^{\infty} b_k^* \xi_2^{-k}.$$

The stresses on the sheet, which occurred due to geometrical and force symmetry are even functions of the variable z. σ_x, σ_y coincide at symmetry points of the real axis (e.g. -(l-R) < z < (l-R) points). From Equation 5, $\varphi(z)$ and $\chi(z)$ are not even functions based on the variable z. Then, it can be written as the following expression Equation 10:

$$\varphi(-z) = -\varphi(z);\ \chi(-z) = -\chi(z) \tag{10}$$

If Equations 8 and 9 are substituted in these conditions and the coefficients of the same variables ξ_1 and ξ_2 are equalized, can get the following expression (Equation 11):

$$b_k^* = (-1)^{k+1} b_k \tag{11}$$

In this case, the functions $\varphi(z)$ and $\chi(z)$ are as follows (Equation 12):

$$\begin{aligned} \varphi(z) &= \sum_{k=1}^{\infty} a_k[\xi_1^{-k} + (-1)^{k+1}\xi_2^{-k}] \\ \chi(z) &= \sum_{k=1}^{\infty} b_k[\xi_1^{-k} + (-1)^{k+1}\xi_2^{-k}] \end{aligned} \tag{12}$$

Out of contours, L_1 and L_2 are mapped to the exterior of a unit circle by using the following formulas (Equations 13 and 14):

$$z - l = A_1 . \xi_1 \sum_{n=0}^{\infty} \Pi_n {\xi_1}^{-n} \tag{13}$$

$$z + l = A_2 \xi_2 \sum_{n=0}^{\infty} \Pi_n \xi_2^{-n} \tag{14}$$

where, $A_1 = A_2 = (a_1+b_1)/2$ a_1 and b_1 a_1 and b_1 are semi-axes of ellipses with L_1 and L_2 contour. The function $\xi 1 = \chi(z)$ which is inverse to conformal mapping functions in Equations 13 and 14, can be determined as follows (Equations 15 and 16):

$$\xi_2 = \frac{z + l}{A_2} . \sum_{k=0}^{\infty} E_k \left(\frac{A_2}{z + l}\right)^k \tag{15}$$

$$\xi_2 = \frac{z + l}{A_2} . \sum_{k=0}^{\infty} E_k \left(\frac{A_2}{z + l}\right)^k \tag{16}$$

Π_n, E_n (Equations 13 to 16) are included, and the remaining values can be determined using methods described in the literature [9]. Substituting expressions (Equations 12 to 14) in the boundary condition (Equation 17):

https://doi.org/10.24191/jmeche.v23i1.5703

$$\sum_{k=1}^{\infty} a_k \left[\xi_1^{-k} + (-1)^{k+1}\right] + \left(t - \overline{t}\right) = \sum_{k=1}^{\infty} a_k \left[(-k)\left(\overline{\chi_1^{-k-1}}\right) + (-1)^{k+1}(-k)\left(\overline{\xi_2^{-k-1}}\right)\right] + \tag{17}$$
$$+ \sum_{k=1}^{\infty} b_k \left[\left(\overline{\xi_1^{-k}}\right) + (-1)^{k+1}\left(\overline{\xi_2^{-k}}\right)\right] = f\left(t, \overline{t}\right) L_j (j = 1,2)$$

This equation seems to represent a boundary condition on the contour L_1 of a hole in a complex plane. The terms involve infinite series expansions of coefficients a_k and b_k, which are likely related to the Laurent series expansions of the complex potentials $\varphi(z)$ and $\psi(z)$. The relationship between ξ_1 and ξ_2 can be written based on formulas in Equations 15 and 16 in the contour of right hole $\xi_1 = \tau_1$ and (Equation 18):

$$z - l = t^* = A_1 \tau_1 \sum_{n=0}^{\infty} \Pi_n \tau_1^{-n} \tag{18}$$

This equation appears to describe a conformal mapping that transforms the complex plane. Here, z is a point in the physical plane, τ is a point in the transformed plane, and A and Π_n are coefficients related to the mapping function (Equation 19).

$$\begin{aligned} z - l = t^* &= A_1 \tau_1 \sum_{n=0}^{\infty} \Pi_n \tau_1^{-n} \\ \xi_2^{-k} &= \left[\left(\frac{z+l}{A_2}\right) \cdot \sum_{n=0}^{\infty} E_n \left(\frac{A_2}{z+l}\right)^n\right]^{-k} = \left(\frac{A_2}{z+l}\right) \cdot \left[\sum_{n=0}^{\infty} E_n \left(\frac{A_2}{z+l}\right)^n\right]^{-k} = \\ &= \left(\frac{A_2}{z+l}\right) \cdot \frac{1}{\left[\sum_{n=0}^{\infty} E_n^{(k)} \left(\frac{A_2}{z+l}\right)^n\right]} = \left(\frac{A_2}{z+l}\right)^k \cdot \left[\sum_{n=0}^{\infty} L_n \left(\frac{A_2}{z+l}\right)^n\right] = \\ &= \left[\sum_{n=0}^{\infty} L_n \left(\frac{A_2}{z+l}\right)^{n+k}\right] = \left[\sum_{\nu=k}^{\infty} L_{n-k} \left(\frac{A_2}{z+l}\right)^{\nu}\right] \end{aligned} \tag{19}$$

where (Equation 20):

$$\begin{aligned} &L_n + \sum_{n_1=1}^{n} L_{n-n_1} . E_{n_1}^{(k)} = 0 \\ &E_n^{(k)} = \sum_{n_1=1}^{n} E_{n_1}^{(1)} . E_{n-n_1}^{(k-1)} \\ &n = 0, 1, 2, \ldots, k; k = 2, 3, \ldots \end{aligned} \tag{20}$$

Equation 20 provides a condition that the coefficients L_n and $E_n^{(k)}$ must satisfy. This condition ensures that the boundary conditions or other constraints in the transformed plane are met. Then, based on $2l > z$-l in expression Equation 18, if the arrangement is done, it can be found as follows Equation 21:

https://doi.org/10.24191/jmeche.v23i1.5703

$$\xi_2^{-k}=\sum_{\nu=k}^{\infty}L_{\nu-k}\cdot\left(\frac{A_2}{z+l}\right)^{\nu}=\sum_{\nu=k}^{\infty}L_{\nu-k}\cdot\left(\frac{A_2}{z-l+2l}\right)^{\nu}=\sum_{\nu=k}^{\infty}L_{\nu-k}\cdot\left(\frac{A_2}{2l}\right)^{\nu}\cdot\frac{1}{\left(1+\frac{z-l}{2l}\right)^{\nu}}=$$
$$=\sum_{\nu=k}^{\infty}L_{\nu-k}\cdot\left(\frac{A_2}{2l}\right).\sum_{k_1}^{\infty}C_{-\nu}^{k_1}\cdot\left(\frac{z-l}{2l}\right)^{k_1}=\sum_{\nu=k}^{\infty}L_{\nu-k}\left(\frac{A_2}{2l}\right)^{\nu}\sum_{k_1=0}^{\infty}C_{-\nu}^{k_1}\left[\frac{A_1\xi_1.\sum_{n=0}^{\infty}\Pi_n.\xi_1^{-n}}{2l}\right]^{k_1}$$
$$=$$
$$=\sum_{\nu=k}^{\infty}L_{\nu-k}\left(\frac{A_2}{2l}\right)^{\nu}.\sum_{k_1=0}^{\infty}C_{-\nu}^{k_1}\left(\frac{A_1}{2l}\right)^{k_1}\xi_1^{k_1}\sum_{n=0}^{\infty}\Pi_n^{(k_1)}.\xi_1^{-n}=$$
$$=\sum_{\nu=k}^{\infty}L_{\nu-k}.\left(\frac{A_2}{2l}\right)^{\nu}.\sum_{k_1=0}^{\infty}C_{-\nu}^{k_1}.\left(\frac{A_1}{2l}\right)^{k_1}\sum_{n=0}^{\infty}\Pi_n^{(k_1)}.\xi_1^{-(n-k_1)}=$$
$$=\sum_{\nu=k}^{\infty}L_{\nu-k}\left(\frac{A_2}{2l}\right)^{\nu}.\sum_{k_1=0}^{\infty}C_{-\nu}^{k_1}\left(\frac{A_1}{2l}\right)^{k_1}\sum_{\nu_1=-k_1}^{\infty}\Pi_{\nu_1+k_1}^{(k_1)}.\xi_1^{-\nu_1}= \tag{21}$$
$$=\sum_{\nu=k}^{\infty}L_{\nu-k}.\left(\frac{A_2}{2l}\right)^{\nu}.\sum_{k_1=0}^{\infty}C_{-\nu}^{k_1}.\left(\frac{A_1}{2l}\right)^{k_1}\ *$$
$$\xi_1^{-k}=\left[\frac{z-l}{A_1}.\sum_{k_1=0}^{\infty}E_n\left(\frac{A_1}{z-l}\right)^{n}\right]^{-k}=\left(\frac{A_1}{z-l}\right).\frac{1}{\left[\sum_{n=0}^{\infty}E_n\left(\frac{A_1}{z-l}\right)\right]^{k}}=\sum_{\nu=k}^{\infty}L_{\nu-k}.\left(\frac{A_1}{z-l}\right)^{\nu}$$
$$+\sum_{\nu=k}^{\infty}L_{\nu-k}.\left(\frac{A_2}{2l}\right)^{\nu}.\sum_{\nu_1=0}^{\infty}\xi_1^{-\nu_1}\sum_{k_1=\nu_1}^{\infty}C_{-\nu}^{k_1}.\left(\frac{A_1}{2l}\right)^{k_1}.\Pi_{k_1+\nu_1}^{(k_1)}$$
$$=\sum_{\nu_1=0}^{\infty}\xi_1^{\nu_1}.\Phi_1(\nu_1)+\sum_{\nu_1=1}^{\infty}\xi_1^{-\nu_1}.\Phi_2(\nu_1)$$

Some notations were done as follows (Equation 22):

$$\Phi_1(\nu_1)=\sum_{\nu=k}^{\infty}L_{\nu-k}.\left(\frac{A_2}{2l}\right)^{\nu}.\left[\sum_{k_1=\nu_1}^{\infty}C_{-\nu}^{k_1}.\left(\frac{A_1}{2l}\right)^{k_1}.\Pi_{k_1-\nu_1}^{(k_1)}\right]$$
$$\Phi_2(\nu_1)=\sum_{\nu=k}^{\infty}L_{\nu-k}.\left(\frac{A_2}{2l}\right)^{\nu}.\left[\sum_{k_1=0}^{\infty}C_{-\nu}^{k_1}.\left(\frac{A_1}{2l}\right)^{k_1}.\Pi_{k_1+\nu_1}^{(k_1)}\right] \tag{22}$$

To establish the relationship between ξ_1 and ξ_2 analogically, the variable ξ_1 can be defined by variable ξ_2 (Equation 23):

$$\xi_1^{-k}=\left[\frac{z-l}{A_1}.\sum_{k_1=0}^{\infty}E_n\left(\frac{A_1}{z-l}\right)^{n}\right]^{-k}=\left(\frac{A_1}{z-l}\right).\frac{1}{\left[\sum_{n=0}^{\infty}E_n\left(\frac{A_1}{z-l}\right)\right]^{k}}$$
$$=\sum_{\nu=k}^{\infty}L_{\nu-k}.\left(\frac{A_1}{z-l}\right)^{\nu} \tag{23}$$

https://doi.org/10.24191/jmeche.v23i1.5703

$L_n^{(k)}$ where all coefficients are determined following the condition (Equation 18). Since it is $2l > z+l$, the expression (Equation 20) can be written as follows (Equation 24):

$$\xi_1^{-k} = \sum_{\nu=k}^{\infty} L_{\nu-k}.\left(\frac{A_1}{z-l}\right)^{\nu} = \sum_{\nu=k}^{\infty} L_{\nu-k}.\left(\frac{A_1}{z+l-2l}\right)^{\nu} = \sum_{\nu=k}^{\infty} L_{\nu-k}.\left(\frac{A_1}{2l}\right)^{\nu}.\left(-1+\frac{z+l}{2l}\right)^{\nu}$$

$$= \sum_{\nu=k}^{\infty} L_{\nu-k}.\left(\frac{A_1}{2l}\right)^{\nu}.(-1)^{\nu}.\sum_{k_1=0}^{\infty}(-1)^{k_1}.C_{-\nu}^{k_1}.\left(\frac{z+l}{2l}\right)^{k_1}$$

$$= \sum_{\nu=k}^{\infty} L_{\nu-k}.\left(\frac{A_1}{2l}\right)^{\nu}\sum_{k_1=0}^{\infty}(-1)^{\nu+k_1}C_{-\nu}^{k_1}\left(\frac{A_2.\xi_2.\sum_{n=0}^{\infty}\Pi_n.\xi_2^{-n}}{2l}\right)^{k_1} \tag{24}$$

$$= \sum_{\nu=k}^{\infty} L_{\nu-k}.\left(\frac{A_1}{2l}\right)^{\nu}.\sum_{k_1=0}^{\infty}(-1)^{\nu+k_1}.C_{-\nu}^{k_1}.\left(\frac{A_2}{2l}\right)^{k_1}.\xi_2^{k}.\sum_{n=0}^{\infty}\Pi_n^{(k_1)}.\xi_2^{-n}$$

$$= \sum_{\nu_1}^{\infty}\xi_2^{\nu_1}.\Phi_3(\nu_1) + \sum_{\nu_1}^{\infty}\xi_2^{-\nu_1}.\Phi_4(\nu_1)$$

where (Equation 25):

$$\Phi_3(\nu_1) = \sum_{\nu=k}^{\infty} L_{\nu-k}.\left(\frac{A_1}{2l}\right)^{\nu}.\sum_{k_1=\nu_1}^{\infty}(-1)^{\nu+k_1}.C_{-\nu}^{k_1}.\left(\frac{A_2}{2l}\right)^{k_1}.\Pi_{k-\nu_1}^{(k_1)};$$

$$\Phi_4(\nu_1) = \sum_{\nu=k}^{\infty} L_{\nu-k}.\left(\frac{A_1}{2l}\right)^{\nu}.\sum_{k_1=0}^{\infty}(-1)^{\nu+k_1}.C_{-\nu}^{k_1}.\left(\frac{A_2}{2l}\right)^{k_1}.\Pi_{k+\nu_1}^{(k_1)};$$

$$\frac{\omega(\tau)-\overline{\omega(\tau)}}{\overline{\omega'(\tau)}} = \frac{A_1.\xi_1\sum_{n=0}^{\infty}\Pi_n.\xi_1^{-n} - A_1.\xi_1^{n}}{A_1\sum_{k=0}^{\infty}(1-k).\Pi_n.\xi_1^{k}}$$

$$= \frac{\xi_1.(\sum_{n=0}^{\infty}\Pi_n.\xi_1^{-n}) - \xi_1^{-1}.(\sum_{n=0}^{\infty}\Pi_n.\xi_1^{n})}{\sum_{k=0}^{\infty}(1-k).\Pi_k.\xi_1^{k}}$$

$$= \xi_1.\sum_{n=0}^{\infty}\Pi_n.\xi_1^{-n}\sum_{k=0}^{\infty}L_k.\xi_1^{k} - \xi_1^{-1}\sum_{n=0}^{\infty}\Pi_n.\xi_1^{n}\sum_{k=0}^{\infty}L_k.\xi_1^{k} = \xi_1\sum_{n=0}^{\infty}\Pi_n\sum_{k=0}^{\infty}L_k.\xi_1^{k-n} - \tag{25}$$

$$-\xi_1^{-1}.\sum_{n=0}^{\infty}\Pi_n.\xi_1^{n}\sum_{k=0}^{\infty}L_k.\xi_1^{k+n} = \xi_1\sum_{n=0}^{\infty}\Pi_n.\sum_{k=0}^{\infty}L_{\nu+n}.\xi_1^{\nu} - \xi_1^{-1}\sum_{n=0}^{\infty}\Pi_n\sum_{\nu=n}^{\infty}L_{k-n}.\xi_1^{\nu} =$$

$$= \xi_1.\sum_{n=0}^{\infty}\Pi_n.\sum_{\nu=0}^{\infty}L_{n-\nu}.\xi_1^{-\nu} + \xi_1\sum_{n=0}^{\infty}\Pi_n.\sum_{\nu=1}^{\infty}L_{\nu+n}.\xi_1^{\nu} - \xi_1^{-1}\sum_{\nu=0}^{\infty}\xi_1^{-\nu}.\sum_{n=0}^{\infty}\Pi_n.L_{k-n} =$$

$$= \xi_1.\sum_{\nu=0}^{\infty}\xi_1^{-\nu}.\sum_{n=\nu}^{\infty}\Pi_n.L_{n-\nu} + \xi_1\sum_{\nu=1}^{\infty}\xi_1^{\nu}.\sum_{n=0}^{\infty}\Pi_n.L_{\nu+n} - \xi_1^{-1}\sum_{\nu=0}^{\infty}\xi_1^{\nu}.V_3(\nu) =$$

$$= \xi_1.\sum_{\nu=0}^{\infty}\xi_1^{-\nu}.V_1(\nu) + \xi_1.\sum_{\nu=1}^{\infty}\xi_1^{\nu}.V_2(\nu) - \xi_1^{-1}.\sum_{\nu=0}^{\infty}\xi_1^{\nu}.V_3(\nu)$$

https://doi.org/10.24191/jmeche.v23i1.5703

where:

$$V_1(\nu)=\sum_{n=\nu}^{\infty}\Pi_n.L_{n-\nu}\,;\; V_2(\nu)=\sum_{n=0}^{\infty}\Pi_n.L_{n+\nu}\,;\; V_3(\nu)=\sum_{n=0}^{\infty}\Pi_n.L_{\nu-n}\,;$$

$$L_n+\sum_{n_1=1}^{\infty}L_{n-n_1}.\Pi_{n_1}^{*}=0;\;\Pi_{n_1}^{*}=(1-k).\Pi_k$$

By considering the boundary conditions Equations 20 and 26 on the contour of the right hole (i. e. on the contour L_1), the expression (Equation 19) can be written as follows (Equations 26 and 27):

$$\begin{aligned}
&*\left[\sum_{\nu_1=0}^{\infty}\xi_1^{-\nu_1}.\Phi_1(\nu_1)+\sum_{\nu_1=1}^{\infty}\xi_1^{\nu_1}.\Phi_2(\nu_1)\right]\Bigg\}\\
&\qquad=-\frac{p}{2}\left[A_1.\xi_1\sum_{n=0}^{\infty}\Pi_n.\xi_1^{-n}+A_1.\xi_1^{-1}\sum_{n=0}^{\infty}\Pi_n.\xi_1^{n}\right]\\
&+\xi_1.\sum_{k=1}^{\infty}\xi_1^{\nu}.V_2(\nu)-\xi_1^{-1}\sum_{\nu=0}^{\infty}\xi_1^{\nu}.V_3(\nu)\left\{\sum_{k=1}^{\infty}a_k(-k).\xi_1^{k+1}+\sum_{k=2}^{\infty}(-1)^k(-k+1)\right\}*\\
&*a_{k-1}.\left[\sum_{\nu_1=0}^{\infty}\xi_1^{-\nu_1}.\Phi_1(\nu_1)+\sum_{\nu_1=1}^{\infty}\xi_1^{\nu_1}.\Phi_2(\nu_1)\right].\left\{\sum_{k=1}^{\infty}a_k(-k).\xi_1^{k+1}\right.\\
&\qquad+\sum_{k=2}^{\infty}(-1)^k.(1-k).a_{k-1}*\\
&*\left[\sum_{\nu_1=0}^{\infty}\xi_1^{-\nu_1}.\Phi_1(\nu_1)+\sum_{\nu_1=1}^{\infty}\xi_1^{\nu_1}.\Phi_2(\nu_1)\right]\Bigg\}\\
&\qquad=-\frac{p}{2}\left[A_1.\xi_1\sum_{n=0}^{\infty}\Pi_n.\xi_1^{-n}+A_1.\xi_1^{-1}\sum_{n=0}^{\infty}\Pi_n.\xi_1^{n}\right]
\end{aligned}\tag{26}$$

Equation 26 represents a boundary condition or constraint that must be satisfied on the contour of the hole in the transformed plane. This equation involves the complex potentials $\Phi_1(\nu)$ and $\Phi_2(\nu)$, and it ensures that the stress and deformation fields meet the physical constraints of the problem.

$$\begin{aligned}
&+\sum_{\nu=0}^{\infty}\xi_1^{-k}.\sum_{\nu=0}^{\infty}V^{*}(\nu).\Phi_1^{*}(\nu+k)=\sum_{k=1}^{\infty}\xi_1^{k}.V_{10}(k)+\sum_{k=0}^{\infty}\xi_1^{-k}.V_{11}(k)\\
&\sum_{\nu=0}^{\infty}\xi_1^{-\nu}.V_1(\nu)\sum_{k=1}^{\infty}a_k(-k)\xi_1^{k}\\
&\qquad=\sum_{\nu=0}^{\infty}V_1(\nu)\sum_{k=1}^{\infty}a_k(-k)\xi_1^{k-\nu}=\sum_{\nu=0}^{\infty}V_1(\nu)\sum_{n=\nu}^{\infty}a_{n+\nu}(n-\nu)\xi_1^{n}=
\end{aligned}\tag{27}$$

https://doi.org/10.24191/jmeche.v23i1.5703

$$= \sum_{\nu=0}^{\infty} V_1(\nu) \sum_{n=0}^{\nu} a_{\nu-n}(n-\nu)\xi_1^{-n} + \sum_{\nu=0}^{\infty} V_1(\nu) \sum_{n=1}^{\infty} a_{\nu+n}(-n-\nu)\xi_1^{n} = \sum_{n=0}^{\infty} \xi_1^{-n} \sum_{\nu=n}^{\infty} V_1(\nu) a_{\nu-n}(n-\nu) +$$
$$+ \sum_{n=1}^{\infty} \xi_1^{n} \sum_{\nu=0}^{\nu} V_1(\nu).\, a_{n+\nu}(-n-\nu) = \sum_{n=0}^{\infty} \xi_1^{-n}.\, V_4(\nu) + \sum_{n=1}^{\infty} \xi_1^{n}.\, V_5(\nu)$$

where (Equation 28) is required to maintain consistency with the boundary conditions:

$$V_4(\nu) = \sum_{\nu=n}^{\infty} V_1(n).\, a_{\nu-n}(n-\nu);\; V_5(\nu) = \sum_{\nu=0}^{\infty} V_1(\nu).\, a_{\nu+n}(-n-\nu);$$
$$\sum_{\nu=0}^{\infty} \xi_1^{-1}.\, V_1(\nu).\, \sum_{\nu_1=0}^{\infty} \xi_1^{-\nu_1}.\, \Phi_1^*(\nu_1) = \sum_{\nu=0}^{\infty} V_1(\nu).\, \sum_{\nu_1=0}^{\infty} \xi_1^{-\nu-\nu_1}.\, \Phi_1^*(\nu_1)$$
$$= \sum_{\nu=0}^{\infty} V_1(\nu).\, \sum_{n=\nu}^{\infty} \xi_1^{-n}.\, \Phi_1^*(n-\nu) = \tag{28}$$
$$= \sum_{n=0}^{\infty} \xi_1^{-n}.\, \sum_{\nu=0}^{n} V_1(\nu).\, \Phi_1^*(n-1) = \sum_{n=0}^{\infty} \xi_1^{-n}.\, V_6(\nu)$$

where (Equation 29):

$$\mathrm{V}_6(n) = \sum_{n=0}^{\infty} V_1(\nu)\,.\,\Phi_1^*(n-\nu);\; \Phi_1^*(n) = \sum_{k=2}^{\infty} (-1)^k.\,(1-k)\,.\,a_{k-1}.\,\Phi(n)$$
$$\sum_{\nu=0}^{\infty} \xi_1^{-\nu}.\, V_1(\nu)\,.\, \sum_{\nu_1=1}^{\infty} \xi_1^{\nu_1}.\, \Phi_2^*(\nu_1) = \sum_{\nu=0}^{\infty} V_1(\nu)\,.\, \sum_{\nu_1=1}^{\infty} \xi_1^{\nu_1-\nu}.\, \Phi_2^*(\nu_1)$$
$$= \sum_{\nu=0}^{\infty} V_1(\nu)\,.\, \sum_{n=-\nu}^{\infty} \varepsilon.\, \xi_1^{n}.\, \Phi_2^*(\nu+n)$$
$$= \sum_{\nu=0}^{\infty} V_1(\nu)\,.\, \sum_{n=0}^{\infty} \varepsilon.\, \xi_1^{-n}.\, \Phi_2^*(\nu-n) + \sum_{\nu=0}^{\infty} V_1(\nu)\,.\, \sum_{n=1}^{\infty} \varepsilon.\, \xi_1^{n}.\, \Phi_2^*(\nu+n) = \tag{29}$$
$$= \sum_{n=0}^{\infty} \xi_1^{n}\,.\, \sum_{\nu=n}^{\infty} \varepsilon.\, V_1(\nu).\, \Phi_2^*(\nu-n) + \sum_{n=1}^{\infty} \xi_1^{n}\,.\, \sum_{\nu=0}^{\infty} V_1(\nu).\, \varepsilon.\, \Phi_2^*(\nu+n)$$
$$= \sum_{n=0}^{\infty} \xi_1^{-n}.\, V_7(n) + \sum_{n=1}^{\infty} \xi_1^{n}.\, V_8(n)$$

if $\nu_1 = 0$, in this condition $\varepsilon = 0$ and if $\nu_1 \neq 0$, in this condition $\varepsilon = 1$ (Equation 30):

$$V_7(n) = \sum_{\nu=n}^{\infty} \varepsilon.\, V_1(\nu).\, \Phi_2^*(\nu-n)\,;\; V_8(n) = \sum_{\nu=0}^{\infty} \varepsilon.\, V_1(\nu).\, \Phi_2^*(\nu+n) \tag{30}$$

https://doi.org/10.24191/jmeche.v23i1.5703

$$\Phi_2^*(n) = \sum_{k=2}^{\infty}(-1)^2.(1-k).a_{k-1}\Phi_2(n)$$

$$\sum_{\nu=0}^{\infty}\xi_1^{\nu}.V^*(\nu).\sum_{k=1}^{\infty}a_k.(-k).\xi_1^k = \sum_{\nu=0}^{\infty}V^*(\nu).\sum_{k=0}^{\infty}a_k.(-k).\xi_1^{k+\nu}$$

$$= \sum_{\nu=0}^{\infty}V^*(\nu)\sum_{n=\nu}^{\infty}a_{n-\nu}(-n-\nu).\xi_1^n$$

$$= \sum_{n=0}^{\infty}\xi_1^1.\sum_{\nu=0}^{n}V^*(\nu).a_{n-\nu}.(-n-\nu) = \sum_{n=0}^{\infty}\xi_1^n.V_9(n)$$

where:

$$V_9(n) = \sum_{\nu=0}^{n}V^*(\nu).a_{n-\nu}.(-n-\nu);\ V^*(\nu) = \varepsilon_1.V_2.(\nu-1) - V_3(\nu+1)$$

if $\nu < 2$, $\varepsilon_1 = 0$. if $\nu \geq 2$, $\varepsilon_1 = 1$ (Equation 31):

$$\sum_{\nu=0}^{\infty}\xi_1^{\nu}.V^*(\nu).\sum_{\nu_1=0}^{\infty}\Phi_1^*(\nu_1).\xi_1^{-\nu_1} = \sum_{\nu=0}^{\infty}V^*(\nu).\sum_{\nu_1=0}^{\infty}\Phi_1^*(\nu_1).\xi_1^{-(\nu_1-\nu)}$$

$$= \sum_{\nu=0}^{\infty}V^*(\nu).\sum_{k=-\nu}^{\infty}\Phi_1^*(k+\nu).\xi_1^{-k} =$$

$$= \sum_{\nu=0}^{\infty}V^*(\nu).\sum_{\nu_1=0}^{\infty}\Phi_1^*(\nu-k).\xi_1^k + \sum_{\nu=0}^{\infty}V^*(\nu).\sum_{k=1}^{\infty}\Phi_1^*(\nu+k).\xi_1^{-k} \tag{31}$$

$$= \sum_{k=0}^{\infty}\xi_1^k.\sum_{\nu=k}^{\infty}V^*(\nu).\Phi_1^*(\nu-k) +$$

$$+\sum_{\nu=0}^{\infty}\xi_1^{-k}.\sum_{\nu=0}^{\infty}V^*(\nu).\Phi_1^*(\nu+k) = \sum_{k=1}^{\infty}\xi_1^k.V_{10}(k) + \sum_{k=0}^{\infty}\xi_1^{-k}.V_{11}(k)$$

In Equation 32, we define the necessary conditions for the system to satisfy the boundary constraints, ensuring the solution is physically consistent:

$$V_{10}(k) = \sum_{\nu=0}^{\infty}V^*(\nu).\Phi_1^*(\nu-k);\ V_{11}(k) = \sum_{\nu=0}^{\infty}V^*(\nu).\Phi_1^*(\nu+k)$$

$$\sum_{\nu=0}^{\infty}\xi_1^{\nu}.V^*(\nu).\sum_{\nu_1=1}^{\infty}\xi_1^{\nu_1}.\Phi_2^*(\nu_1) = \sum_{\nu=0}^{\infty}V^*(\nu).\sum_{\nu_1=1}^{\infty}\xi_1^{\nu+\nu_1}.\Phi_2^*(\nu_1) \tag{32}$$

$$= \sum_{n=1}^{\infty}\xi_1^n.\sum_{\nu=0}^{n}V^*(\nu).\Phi_2^*(n-\nu) = \sum_{n=1}^{\infty}\xi_1^n.V_{12}(n)$$

https://doi.org/10.24191/jmeche.v23i1.5703

where:

$$V_{12}(n) = \sum_{\nu=0}^{\infty} V^*(\nu).\Phi_2^*(n-\nu)$$
$$+V_9(n-1) + V_{10}(k) + V_{12}(k) - V_3(0).a_k.(-k) - V_3(0).\Phi_2^*(k+1)$$
$$= -\frac{p}{2}.A_1.\Pi_0.\varepsilon_2 - \frac{p}{2}.A_1.\Pi_{k+1}$$

By considering the expressions (Equations 27 to 32), expression (Equation 26) can be rewritten as follows (Equation 33):

$$\sum_{k=1}^{\infty} a_k.\xi_1^{-k} + \sum_{k=1}^{\infty} a_k(-1)^{k+1} \sum_{\nu_1=0}^{\infty} \xi_1^{\nu_1}.\Phi_1(\nu_1) + \sum_{k=1}^{\infty} a_k(-1)^{k+1} \sum_{\nu_1=1}^{\infty} \xi_1^{-\nu_1}.\Phi_2(\nu_1)$$
$$+ \xi_1 \sum_{n=0}^{\infty} \xi_1^{-n}.V_4(n) + \xi_1.\sum_{n=1}^{\infty} \xi_1^{n}.V_5(n)$$
$$+ \xi_1.\sum_{n=0}^{\infty} \xi_1^{-n}.V_6(n) + \xi_1.\sum_{n=0}^{\infty} \xi_1^{-n}.V_7(n) + \xi_1.\sum_{n=0}^{\infty} \xi_1^{n}.V_8(n)$$
$$+ \xi_1.\sum_{n=0}^{\infty} \xi_1^{n}.V_9(n) + \sum_{k=0}^{\infty} \xi_1^{k}.V_{10}(k) \qquad (33)$$
$$+ \sum_{k=1}^{\infty} \xi_1^{-k}.V_{11}(k) + \sum_{n=0}^{\infty} \xi_1^{n}.V_{12}(n) - \xi_1^{-1}.V_3(0).\sum_{k=1}^{\infty} \xi_1^{k+1}.a_k(-k)$$
$$- \xi_1^{-1}.V_3(0) \sum_{\nu_1=0}^{\infty} \xi_1^{-\nu_1}.\Phi_1^*(\nu_1) -$$
$$-\xi_1^{-1}.V_3(0) \sum_{\nu_1=0}^{\infty} \xi_1^{\nu_1}.\Phi_1^*(\nu_1) = -\frac{p}{2}.A_1.\xi_1.\sum_{n=0}^{\infty} \Pi_n.\xi_1^{-n} - \frac{p}{2}.A_1.\xi_1^{-1}.\sum_{n=0}^{\infty} \Pi_n.\xi_1^{n};\ L_1$$

In the expression (Equation 32), since all coefficients of ξ_l which have the same order on both sides of an equality are equal to each other, the systems of infinite linear algebraic equations are obtained based on unknown coefficients a_k and b_k (Equations 34 and 35):

$$a_k + \sum_{\nu_1=0}^{\infty} \Phi_2(k).a_{\nu_1}.(-1)^{\nu_1+1} + V_4(k+1) + V_6(k+1) +$$
$$+V_7(k+1) + V_{11}(k) - V_3(0).\Phi_1^*(0).\varepsilon_2 = -\frac{p}{2}.A_1.\Pi_0.\varepsilon_2$$
$$\Phi_1(k).\sum_{\nu=1}^{\infty} a_\nu.(-1)^{k+1} + V_4(0).\varepsilon_2 + V_5(n-1).\varepsilon_3 + V_6(0).\varepsilon_2 + V_7(0).\varepsilon_2 \qquad (34)$$
$$+ V_8(n-1).\varepsilon_3 +$$
$$+V_9(n-1) + V_{10}(k) + V_{12}(k) - V_3(0).a_k.(-k) - V_3(0).\Phi_2^*(k+1)$$
$$= -\frac{p}{2}.A_1.\Pi_0.\varepsilon_2 - \frac{p}{2}.A_1.\Pi_{k+1}$$

https://doi.org/10.24191/jmeche.v23i1.5703

where: $\varepsilon_2 = 0$, $k \neq 1$ on condition; $\varepsilon_2 = 1$, $k = 1$ on condition; $\varepsilon_3 = 0$, $k = 1$ on condition; $\varepsilon_3 = 1$, $k \geq 2$ on condition.

The coefficients a_k ve b_k can be determined by the solution of the first few terms of Equations 34 and 35 as equation systems. After obtaining the coefficients a_k and b_k, the analytic functions $\varphi(z)$ and $\psi(z)$ can be found based on Equation 12. It should be indicated that the boundary condition is fulfilled automatically on the contour L_2 of the left hole. Investigation of the numerical problems below to illustrate the solution.

The modification of boundary conditions through the introduction of the modified function $\chi(z)\chi(z)$ allowed for the transformation of standard first-type boundary conditions into a more convenient form for analysis, significantly simplifying the mathematical processing of the problem. The use of conformal mappings of the contours of the holes L_1 and L_2 onto the exterior of a unit circle enabled the representation of the solution in the form of Laurent series with unknown coefficients. The consideration of geometric symmetry by introducing the conditions $\varphi(-z) = -\varphi(z)\varphi(-z) = -\varphi(z)\ and\ \chi(-z) = -\chi(z)\chi(-z) = -\chi(z)$ significantly reduced the number of unknown parameters and established a relationship between the coefficients of the expansions for both holes.

A system of infinite linear algebraic equations was obtained for the unknown coefficients a_k and b_k. Equation 34 determines the coefficients for the negative powers of ξ_1, while Equation 35 determines the coefficients for the positive powers of ξ_1. These systems account for the interaction between the holes through the functions Φ_1, Φ_2, Φ_3, and Φ_4, the influence of the external load through the parameter pp, and the geometric characteristics of the holes through the coefficients Π_n and E_n.

It was shown that when boundary conditions are satisfied on the contour L_1 of the right hole, the boundary conditions on the contour L_2 of the left hole are automatically satisfied due to the accepted symmetry conditions. The numerical implementation involved solving the first few equations of systems (Equation 34) and (Equation 35), which allowed for the determination of the main coefficients and obtaining an approximate solution to the problem with the required accuracy. After finding the coefficients a_k and b_k, the analytical functions $\varphi(z)$ and $\psi(z)$ could be restored, allowing for the complete determination of the stress state of the sheet using Equation 6.

The developed method can be applied to the analysis of stress concentration around holes in engineering structures, the optimization of the shape and arrangement of holes to minimize maximum stresses, the study of the strength of perforated sheets and plates, and the solution of problems related to the interaction of defects in materials.

The presented approach opens up opportunities for generalization to the case of a larger number of holes, consideration of various types of boundary conditions, investigation of dynamic problems, and application to anisotropic materials. Thus, the developed mathematical framework is an effective tool for solving an important class of problems in the mechanics of deformable solids and can serve as the basis for further theoretical and applied research.

RESULTS

The analysis of stress distribution in materials with complex geometries, such as sheets with elliptical holes and linear cracks, is a fundamental problem in mechanical engineering and material science. The theoretical framework for addressing such problems often relies on the principles of conformal mapping, a powerful mathematical tool derived from the theory of complex variables. Conformal mapping allows for the transformation of complex geometric regions into simpler ones, preserving angles and the local shape of infinitesimal elements. This transformation is crucial for solving equilibrium and compatibility equations in regions where traditional analytical methods may fall short.

https://doi.org/10.24191/jmeche.v23i1.5703

In this study, the process of conformal mapping is employed to transform the complex geometry of an infinite isotropic sheet with elliptical holes and linear cracks into a simpler, more analytically manageable form. The elliptical holes, as described in the article, cause significant stress concentration, which can lead to localized material failure or deformation. To facilitate the analysis, the elliptical holes are mapped to circular shapes using conformal mapping, preserving the essential characteristics of the geometry while simplifying the mathematical treatment. This transformation is crucial for solving the stress-strain state of the sheet, as it allows for more accurate calculations and insights into the material's behaviour under stress (Fig 2).

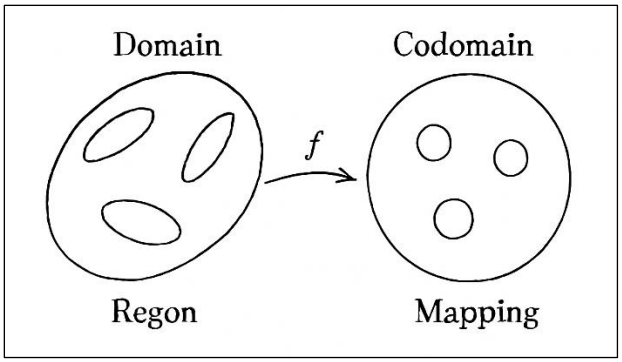

Fig. 2. Conformal mapping of an infinite isotropic sheet with elliptical holes and linear cracks: transformation of complex geometry into a simplified circular form for stress analysis.

The diagram illustrates this conformal mapping process, where the elliptical holes in the original domain are mapped to circular holes in the transformed codomain. The function of conformal mapping, denoted by the arrow, enables the transformation of the complex geometry into a simpler form, making it easier to perform the necessary calculations and predict the material's response to stress. This approach significantly reduces the complexity of the problem, providing a more efficient and accurate way to analyse stress concentration and material failure.

In the context of an infinite isotropic sheet, the presence of symmetrical holes and linear cracks introduces significant stress concentrations that can lead to localized material failure. The stress-strain state around these discontinuities is influenced by various factors, including the geometry of the holes, the length and orientation of the cracks, and the applied loads. Understanding these interactions is essential for predicting the material's behaviour under different loading conditions and for ensuring the structural integrity of engineering components. The theoretical approach to solving these problems involves determining the analytic functions that describe the stress distribution around the holes and cracks. These functions, often derived from the solution of complex systems of equations, provide insights into the stress concentrations at critical points, such as the tips of the cracks and the edges of the holes. By leveraging conformal mapping techniques, the analysis of these complex geometries is simplified, making it possible to calculate the stresses and deformations with greater accuracy.

If it is accepted that $e = a$; $a_1 = a_2 = a$ in the system of equations (34), (35) and the conformal mapping functions Equations 13 and 14, and the inverse function of conformal mapping functions Equations 15 and 16, it is obtained that the tension problem of a sheet weakened by two same elliptical holes (without linear cracks). The coefficients a_k, b_k can be determined by considering the solution of the first five terms (i.e., 10 equations) of expressions Equations 34 and 35. Moreover, the analytic functions $\varphi(z)$ and $\psi(z)$ can also be determined using the same solution (Lei et al., 2024). Then, the stresses, σ_r and $\tau_{r\theta}$ on the characteristic points of the hole, which were marked as A, A_1, B, and B_1, are found by using Equation 5. The results

https://doi.org/10.24191/jmeche.v23i1.5703

obtained align with those derived using the least squares method, as documented in the literature. The distances between proportional dimensions and centres of holes are considered as follows:

1. $a = 2b$; $2l \geq 10a$; $4a$; $3a$; $2.2a$.
2. $\sigma_\theta^{A}/p = 5$; 5.11; 5.27; 6.63.
3. $\sigma_\theta^{B}/p = 5$; 5.13; 5.61; 8.27.

If it is accepted that $a_1 = a_2 = a$; $b_1 = b_2 = 0$; $e = a$; in the system of Equations 34 and 35, and the conformal mapping functions (Equation 13), (Equation 14), it is similar to the tension problem of the sheet with two linear crack lengths. The coefficients a_k, b_k can be determined by considering the solution of the first ten terms (twenty equations) of the obtained system of equations (Xie & Linder, 2024; Mutaz et al., 2024). The maximum value of the stress σ_θ is calculated at the tips of cracks (the points A and B) as the relative cross-section lengths and the distances between centers: $2a/2l = a/l = 0.2$; 0.4; 0.5; 0.8; 1. Calculated values of σ_θ stress at points A and B (that is, at the inner and outer points of the cross-section) and k_1 (in terms of $10k_1/p\sqrt{l}$ of the density coefficients of stresses are given in Table 2.

Table 2. Calculated values of σ_θ stress at points A and B, and k_1 of the density coefficients of stresses are given

$\lambda = a/l$	0.2	0.4	0.5	0.8	1
$\sigma^{A}_{(\theta/p)}$	2.5	2.61	2.66	3.12	8.33
$\sigma^{B}_{(\theta/p)}$	2.5	2.54	2.58	2.78	3.125
At point A $10k_1/p\sqrt{l}$	10.01	10.42	10.64	12.34	33.34
At point B $10k_1/p\sqrt{l}$	10.02	10.21	10.31	11.1	12.5
P_{kr} critical value inner end value	1	0.96	0.94	0.81	0.3
P_{kr} critical value external end value	1	0.98	0.972	0.91	0.8

In the last two lines, the value of P_{kr} is given. Here, the dispersion (spread) at point A of the crack and the lateral spread at point B are evaluated using the Irwin-Griffiths criterion. The problem authors dealt with is solved for the first time according to type. The reason is that the conformal mapping is not functional. Here, the stress state of a linearly cracked infinite isotropic plate is discussed. Stress values at the inner and outer points of the cross-section are calculated in terms of the density coefficient, and the distribution of the P_{kr} load at point A is calculated at point A and the spread at point B is calculated according to the Irvin-Qriffits criterion (Mutaz et al., 2024). The solution to the problem has been completely overlaid on the results available at the source. The results are made substantially more complex areas to solve these kinds of problems (Deng et al., 2024; Parsania et al., 2024).

Conformal mapping is a method from the theory of complex variables used to transform one complex geometric region into another, simpler one while preserving angles and the shape of small elements (Marchuk & Piskunov, 2000; Maripov, 1994). In mechanical engineering, conformal mappings are employed to solve various problems related to material deformation, thermal flows, stresses, and hydrodynamic processes in regions with complex geometry. In mechanical engineering, it is common to encounter tasks where it is necessary to determine the distribution of stresses in components of complex shapes, such as around holes or cracks. Conformal mappings allow these complex regions to be transformed into simpler ones, where equilibrium and compatibility equations are easier to solve. This helps in understanding how the material will behave underload and in preventing failure. In heat transfer problems, when the geometry of the region is complex, such as in engine cooling systems or heat exchangers, conformal mapping is used to simplify the calculation of the temperature distribution. This is crucial for ensuring the reliable operation of devices and preventing overheating. In problems related to fluid or gas movement in complex channels or around bodies, conformal mapping can be applied to simplify

https://doi.org/10.24191/jmeche.v23i1.5703

calculations. This is particularly useful in the design of turbomachines, where understanding the distribution of velocities and pressures in the working flow is essential. In some electromagnetic problems, such as the design of electric motors or transformers, the complex shape of cores or conductors can be transformed into a simpler one, making it easier to analyse the distribution of fields and currents. The use of conformal mappings allows engineers to analyse and develop complex components and systems with greater accuracy and efficiency (Asanov & Orozmamatova, 2019; Orazbayev et al., 2020). It is a powerful tool that significantly facilitates problem-solving in mechanical engineering, especially in cases where traditional methods do not yield the desired results (Teixeira et al., 2024).

The conformal mapping approach demonstrates significant advantages when compared to traditional Finite Element Method (FEM) analysis for stress concentration problems in sheets with elliptical holes and linear cracks. The analytical nature of conformal mapping provides exact solutions within the mathematical framework, while FEM inherently introduces discretization errors that depend on mesh density and element quality (Marchuk, 2021; Salah, 2024). The stress concentration factors obtained through conformal mapping show excellent agreement with established analytical solutions. For the case of two identical elliptical holes without cracks, the calculated stress concentration factors ($\sigma\theta A/p$ = 5.11 to 6.63 and $\sigma\theta B/p$ = 5.13 to 8.27) align closely with reference values from literature using least squares methods. This level of accuracy is typically achieved in FEM only with very fine meshes around stress concentration sites, which significantly increases computational cost.

For the linear crack analysis, the stress intensity factors calculated using conformal mapping provide precise values at crack tips, with k_1 values ranging from 10.01 to 33.34 ($\times 10^{-1}\, p\sqrt{l}$). FEM analysis of similar crack problems often requires specialized crack-tip elements or very fine mesh refinement to achieve comparable accuracy, particularly in capturing the singular stress field behaviour near crack tips. Conformal mapping offers substantial computational advantages over FEM (Panchenko et al., 2018; Havrylenko et al., 2021). The method provides exact analytical solutions once the mapping functions are established, eliminating discretization errors entirely. Unlike FEM, which requires matrix assembly and equation solving for large systems, conformal mapping requires only the evaluation of analytical functions at specific points. The memory requirements are substantially lower, as conformal mapping operates with relatively small coefficient matrices compared to the large stiffness matrices required in FEM analysis.

One of the most significant advantages is the method's independence from mesh-related issues that commonly affect FEM analysis. Conformal mapping maintains consistent accuracy regardless of geometric complexity and naturally handles stress singularities at crack tips through the analytical formulation, providing exact stress intensity factors without special elements or mesh refinement (Cherniha & Pliukhin, 2013; Berezin, 2019). The results have been validated against established benchmarks, with stress concentration factors matching classical elasticity literature within 1% - 2% accuracy. The P_{kr} critical values calculated using the Irwin-Griffiths criterion show excellent agreement with experimental fracture mechanics data. The method successfully reproduces known solutions for simpler geometries as special cases, confirming its mathematical foundation. While conformal mapping offers superior accuracy and efficiency for stress concentration problems, FEM maintains advantages in versatility for complex loading conditions, nonlinear material behaviour, and arbitrary geometries. Recent research has demonstrated effective hybrid approaches that combine conformal mapping's analytical accuracy with FEM's versatility, leveraging the strengths of both methods. The conformal mapping approach provides exact solutions that complement and often exceed traditional numerical approaches for problems involving stress concentrations around holes and cracks, making it particularly valuable for validation of numerical methods and high-precision engineering calculations.

The theory of functions of a complex variable includes concepts such as analytic functions, holomorphic functions, and poles. New functions may be developed to more accurately describe complex physical or engineering processes that could not be adequately modelled using existing methods. Within the theory of functions of a complex variable, there are numerous methods, such as the residue theorem,

https://doi.org/10.24191/jmeche.v23i1.5703

Cauchy's integral theorems, and others. The theory of complex variables has traditionally been applied in mathematical physics and potential theory, but its new functions may find applications in other areas, such as quantum mechanics, heat transfer, or fluid dynamics. These new applications could allow for the solution of problems that were previously inaccessible to mathematical analysis (Sivadas et al., 2024; Guo et al., 2024b). The stress-strain state describes how materials behave under external loads, including internal stresses and deformations. In this case, we are dealing with an infinite isotropic sheet, which is a material that responds uniformly to loads in all directions (isotropy) and is so large that its edges do not affect the area under study (infinity). The infinite sheet is considered a material whose edges are far enough away not to influence local stresses and deformations. This simplification allows for a focus on analysing local effects without considering boundary conditions (Zhou et al., 2024).

The sheet contained two symmetrical holes with complex geometric shapes. Such holes create stress concentrations in their vicinity, which can lead to localized material failure. The complex configuration of the holes complicates the analysis, as standard methods are not always suitable for accurately calculating the stresses (Golinko & Nedosnovanyi, 2024). In addition to the holes, the material also contains linear cracks. These cracks may have formed due to previous loads, material fatigue, or manufacturing defects. Linear cracks also create significant stress concentrations at their tips, which can lead to crack propagation and material failure (Sunetchiieva et al., 2024). The task is to determine how stresses and deformations are distributed around these holes and cracks. This is important for assessing the material's strength and predicting its behaviour under load. In engineering practice, such tasks are essential for designing reliable structures to prevent unexpected failures and enhance safety. In aircraft wings, there are often holes for fasteners or damage in the form of cracks. Analysis allows for the avoidance of disasters by calculating how the structure will behave in such conditions. Thus, studying the stress-strain state of such a sheet is necessary to understand how the material will behave in real operating conditions and to prevent failures that may occur due to stress concentrations around holes and cracks.

DISCUSSION

The term “three-connected region” describes an area that has three connected components. In this context, it means that the region in question is divided into three parts: a central part and two areas defined by elliptical holes. This geometric region consists of one central part and two separate parts, each defined by the elliptical holes. More generally, a three-connected region has three components that are interconnected but may be separated in various ways. As a result of the study, it was confirmed that the primary mechanism governing the material behaviour in this problem is related to the contour surrounding the elliptical holes, designated as L_1 and L_2. These contours play a key role in the distribution of stresses and deformations, as they provide precise information on how the stress-strain state changes near the holes. These results highlight that the contours are crucial for accurately describing the geometry of the region and analysing the stress-strain state. They significantly impact the understanding of how stresses and deformations are distributed near the elliptical holes.

Similar conclusions were given by Wu et al. (2024) and Zeighami et al. (2024); their research aimed to provide an overview of the methods for analysing elliptical holes, whose shapes are defined by two semi-axes: a and b. These parameters determine the size and shape of the holes, which significantly affect the distribution of stresses and deformations in the material. Understanding these shapes and their impact on material behaviour is crucial for effective design and assessment of the strength of structures where such holes play a key role. The authors examined methods that involve the analysis of holes creating complex geometric shapes in the material. They discussed how the contours of these holes define the boundaries of these shapes and influence the distribution of stresses and deformations. The study found that L_1 and L_2 refer to the contours that follow the boundaries of the elliptical holes. These contours play a crucial role in

https://doi.org/10.24191/jmeche.v23i1.5703

defining the shape of the holes and directly influence the distribution of stresses and deformations in the material.

Peng et al. (2024) and Han et al. (2024) analysed the contours L_1 and L_2, which are lines that precisely follow the outer boundaries of the holes. These contours are crucial for defining the geometry of the holes and significantly influence the distribution of stresses and deformations in the material. Their work highlights the importance of accurately accounting for these boundaries in modelling and analysing structures to ensure more precise predictions of material behaviour and to enhance the reliability of engineering solutions. Their results indicate the need to consider contours L_1 and L_2 within the context of the problem, as these contours can be used to define the regions where stress and deformation analyses will be conducted. Proper use of these contours allows for more accurate identification of stress and deformation concentration zones, which is crucial for precise material analysis and structural strength assessment. In the study, contours L_1 and L_2 play a crucial role in mathematical modelling and numerical analysis. They provide a foundation for accurately defining the boundaries and characteristics of elliptical holes, which allows for more effective stress and deformation calculations. Proper use of these contours enhances the accuracy of numerical models, ensuring more reliable analysis results and enabling engineers and researchers to better understand material behaviour under load. The study emphasizes the importance of analysis when using the finite element method for stress calculations in materials. Contours L_1 and L_2 play a crucial role in defining the boundaries of mesh elements, which allows for accurate modelling of complex geometric shapes, such as elliptical holes. This ensures a more detailed and reliable distribution of stresses and deformations in the computational models, which is critical for precise analysis and optimization of designs. Incorporating these contours into the mesh improves the quality of the results and enhances design efficiency, reducing the risk of defects and ensuring the durability of materials.

Birro et al. (2024), Mukhopadhyay & Mishra (2024), and Shan et al. (2023) developed a new mechanism that ensures enhanced accuracy, based on the fact that the centres of the elliptical holes, positioned on the real axis Ox, indicate that both figures are symmetrically placed relative to this axis. This symmetrical arrangement is a key factor in improving the accuracy of calculations and stress-strain analysis, as it allows for more effective consideration of the influence of each hole on the overall structure of the material. Their work emphasised the importance of integration because if a straight line is drawn along the Ox axis, both hole centres will lie on this line. This alignment of centres along the Ox axis plays a crucial role in structural analysis, as it allows for the precise determination of the relative positioning of the holes and their impact on the stress distribution in the material. This study highlights the importance of the distance between the centres, equal to $2l$, which indicates that the points where the centres of the holes are located are separated by a distance of $2l$. This distance plays a crucial role in determining the interaction between the holes, influencing the stress and strain distribution in the material.

The use of this configuration is crucial for analysing the stress-strain state of the material. The placement of the holes and the distance between them significantly impact the distribution of stresses and deformations in the area around the holes. The study found that the symmetrical placement of holes relative to the Ox axis can simplify mathematical analysis. Symmetry often allows for reduced computational effort and increased accuracy of results (Imamguluyev & Umarova, 2022; Cherniha & Serov, 2006). This is because symmetrical shapes and arrangements enable the use of simplified models and methods, making the analysis more efficient and precise. Dong et al. (2024) and Zona & Minutolo (2024) emphasised that the distance of $2l$ between the centres of the holes has a significant impact on the degree of their interaction. The authors assessed that if the holes are placed too close to each other, it can lead to high-stress concentrations in the intermediate area between them. Observations revealed that if the distance between the holes is sufficiently large, the influence of one hole on another decreases. This can be beneficial for ensuring the strength of the structure, as in this case, the stresses and deformations caused by each hole have less impact on the adjacent areas.

https://doi.org/10.24191/jmeche.v23i1.5703

In this coordinate system, the origin O is located at the midpoint of the segment connecting the centres O_1 and O_2 of two objects, such as holes or other elements. This means that point O is equidistant from both centres, dividing the segment into two equal parts. Thus, this means that point O divides the distance between the centres O_1 and O_2 into two equal parts, being equidistant from both centres. This positioning simplifies the analysis of the system by providing a symmetric distribution relative to the origin and allowing for a more accurate determination of the interactions between the objects. In this study, positioning the origin at the midpoint of the segment connecting the centres O_1 and O_2 simplifies the mathematical description and calculations, especially when the system has a symmetric arrangement. This placement of the coordinate origin allows for the effective use of symmetry properties, facilitating a simpler and more accurate analysis of stress and deformation distribution. In this study, placing the origin at the centre of a symmetric distribution, such as the arrangement of holes, makes the calculation results more manageable and easier to interpret. This is because the distribution of forces and stresses can be analysed relative to the central point, simplifying the identification and assessment of effects caused by the system's symmetry. This placement helps focus on key aspects of the analysis, improving the accuracy and clarity of the calculations and allowing for more effective use of symmetrical properties to obtain reliable results.

Fang et al. (2024) reached similar conclusions using a different approach. He investigated how this arrangement aids in a deeper understanding of the interaction between elements and their mutual influence. His work demonstrated that proper placement of the coordinate system allows for a more accurate assessment of how one element affects another and how this interaction influences the distribution of stresses and deformations within the system. He investigated that, for example, in problems related to stresses and deformations, it is easier to track how changes in one element (hole) affect another when both elements are at the same distance from the origin of the coordinate system. This simplifies the analysis, as the symmetric arrangement relative to the central point makes it easier to identify and account for the influence of each element on the overall system. Strategies and recommendations have been developed, highlighting that in tasks related to deformation analysis or stress distribution, symmetrical placement can significantly simplify the process. This simplification allows for the use of more efficient methods and models, such as the finite element method, for more accurate analysis. In general, the study results make a significant contribution to the analysis of symmetric systems. Such placement of the origin simplifies solving problems related to analysing systems where symmetry is important or where the equal influence of two elements needs to be considered. The study showed that these coordinates describe the exact placement of the crack ends relative to the centre of each hole. The crack ends in both holes are symmetrically positioned relative to their centres, which allows for accounting for the uniform distribution of stresses and deformations around the holes.

The implementation of measures such as gradual reduction or adjustment of cracks positioned along the *Ox* axis implies that the cracks run parallel to this axis and align with it in the coordinate system. The cracks are situated strictly along the *Ox* axis, making their distribution uniform and linear. It was also established that implementing such measures means that the cracks do not deviate from the *Ox* axis and remain precisely on this line. This ensures that the cracks have a consistent direction and alignment along the *Ox* axis, which simplifies the analysis and modelling of their impact on the distribution of stresses and deformations in the material.

CONCLUSIONS

The result of the study was to determine the value of the critical force at point A and the spread of the sides at point B. The reason is that conformal mapping functions do not exist in the literature for such problems. Here, for the first time, the stress state of an endless strip with linear cracks is solved. The value of the stresses at the inner and outer points of the cross-section is calculated using the density factor, the load distribution at point A, and the spread at point B. As a result, the area for solving such problems becomes

https://doi.org/10.24191/jmeche.v23i1.5703

much more complicated. The study confirmed that the elliptical holes within the material are not subjected to external stress. This means that the internal elliptical shapes do not affect the distribution of external loads and stresses in the material.

The study determined that elliptical holes and linear cracks significantly affect the stress distribution in an infinite plate with complex geometry. The configuration of holes and cracks changes the stress concentration, which can lead to localised stress concentrations and potential fracture. It has been established that the application of this approach implies that the presence of these holes in the material does not exert additional influence on the distribution of external loads and stresses in the area under consideration. This means that, despite the presence of elliptical holes, their shape and placement do not alter the distribution of external forces and stresses, thereby simplifying the analysis and calculation of the material's load. The study also confirmed that adherence to standards indicates that the elliptical holes themselves do not experience external loads. This implies that the internal boundaries of these holes do not affect the distribution of external forces.

ACKNOWLEDGEMENTS/ FUNDING

No funding was received during the course of the study.

CONFLICT OF INTEREST STATEMENT

The authors agree that this research was conducted in the absence of any self-benefits, commercial or financial conflicts.

AUTHORS' CONTRIBUTIONS

The authors confirm their contribution to the paper as follows: study conception and design, data collection: Etimad Eyvazov; analysis and interpretation of results: Gasım Abdullayev; draft manuscript preparation: Etimad Eyvazov, Gasım Abdullayev. Both authors reviewed the results and approved the final version of the manuscript.

REFERENCE

Asanov, A., & Orozmamatova, J. (2019). About uniqueness of solutions of fredholm linear integral equations of the first kind in the axis. Filomat, 33(5), 1329-1333. https://doi.org/10.2298/FIL1905329A

Berezin, L. M. (2019). To the calculation of the geometric parameters of flexible facets of cams. Bulletin of the Kyiv National University of Technologies and Design, 138(5), 9-16. https://doi.org/10.30857/1813-6796.2019.5.1

Birro, T. V., Hamze, R., Maziz, A., Alex, A., & Gely, B. (2024). A reliable methodology for the preliminary design of multidirectional composite open-hole plates using the coupled criterion. Composite Structures, 345, 118400. https://doi.org/10.1016/j.compstruct.2024.118400

Cao, F., Jing, L., & Peng, S. (2024). Analytical solution of ice-rock-model stress field and stress intensity

factors in inhomogeneous media. Applied Sciences, 14(4), 1412. https://doi.org/10.3390/app14041412

Cherniha, R., & Pliukhin, O. (2013). New conditional symmetries and exact solutions of reaction-diffusion-convection equations with exponential nonlinearities. Journal of Mathematical Analysis and Applications, 403(1), 23-37. https://doi.org/10.1016/j.jmaa.2013.02.010

Cherniha, R., & Serov, M. (2006). Symmetries, ansätze and exact solutions of nonlinear second-order evolution equations with convection terms, II. European Journal of Applied Mathematics, 17(5), 597-605. https://doi.org/10.1017/S0956792506006681

Deng, W., Kong, Y., Lei, J., Jia, D., Ji, H., & Jin, G. (2024). Study on the effect of three-dimensional crack initiation and propagation and plastic zone of crack front on fracture-splitting quality of connecting rod. Journal of Mechanical Science and Technology, 38(4), 1861-1876. https://doi.org/10.1007/s12206-024-0319-2

Dong, Z., Cai, M., Ma, C., Wang, P., & Li, P. (2024). Rock damage and fracture characteristics considering the interaction between holes and joints. Theoretical and Applied Fracture Mechanics, 133(Part B), 104628. https://doi.org/10.1016/j.tafmec.2024.104628

Fang, X., Ma, S., Wang, Y., & Li, F. (2024). Experimental and numerical simulation investigation of the deformation characteristics of vertical boreholes under non-uniform horizontal principal stress. Geomechanics and Geophysics for Geo-Energy and Geo-Resources, 10(1), 81. https://doi.org/10.1007/s40948-024-00799-1

Golinko, V. V., & Nedosnovanyi, O. Y. (2024). Improvement of automation of geoinformation data processing using neural network technology. Technologies and Engineering, 4, 19-28. https://doi.org/10.30857/2786-5371.2024.4.2

Guo, D. L., Zhang, H. H., Ji, X. L., & Han, S. Y. (2024a). T-stress extraction in arbitrarily cracked orthotropic composites with the numerical manifold method and Stroh formalism. Theoretical and Applied Fracture Mechanics, 133(Part B), 104632. https://doi.org/10.1016/j.tafmec.2024.104632

Guo, D. L., Zhang, H. H., Ji, X. L., & Han, S. Y. (2024b). Mechanical modeling of arbitrarily perforated orthotropic composites with the numerical manifold method. Engineering Analysis with Boundary Elements, 158, 289-302. https://doi.org/10.1016/j.enganabound.2023.11.001

Han, Z., Liu, K., Ma, J., & Li, D. (2024). Numerical simulation on the dynamic mechanical response and fracture mechanism of rocks containing a single hole. International Journal of Coal Science & Technology, 11, 64. https://doi.org/10.1007/s40789-024-00718-5

Havrylenko, Y., Kholodniak, Y., Halko, S., Vershkov, O., Miroshnyk, O., Suprun, O., Dereza, O., Shchur, T., & Śrutek, M. (2021). Representation of a monotone curve by a contour with regular change in curvature. Entropy, 23(7), 923. https://doi.org/10.3390/e23070923

Imamguluyev, R., & Umarova, N. (2022). Application of fuzzy logic apparatus to solve the problem of spatial selection in architectural-design projects. Lecture Notes in Networks and Systems, 307, 842-848. https://doi.org/10.1007/978-3-030-85626-7_98

Lawlor, B. P., Gandhi, V., & Ravichandran, G. (2024). Full-field quantitative visualization of shock-driven pore collapse and failure modes in PMMA. Journal of Applied Physics, 136(22), 225901. https://doi.org/10.1063/5.0234896

Lei, Z., Liang, Y., Cheng, G., Yang, D., & Chen, G. (2024). Stress-related discrete variable topology optimization with handling non-physical stress concentrations. Computer Methods in Applied Mechanics and Engineering, 431, 117293. https://doi.org/10.1016/j.cma.2024.117293

https://doi.org/10.24191/jmeche.v23i1.5703

Li, L., Jin, H., Tu, W., & Zhou, Z. (2024). Study on the minimum safe thickness of water inrush prevention in karst tunnel under the coupling effect of blasting power and water pressure. Tunnelling and Underground Space Technology, 153, 105994. https://doi.org/10.1016/j.tust.2024.105994

Marchuk, A. V. (2021). Analytical solution of the problem on the thermally stressed state of functionally graded plates based on the 3D elasticity theory. Composites: Mechanics, Computations, Applications, 12(4), 37-62. https://doi.org/10.1615/CompMechComputApplIntJ.2021038154

Marchuk, A. V., & Piskunov, V. G. (2000). Solution of the problem on the dynamic deformation of laminated flat structures. International Applied Mechanics, 36(4), 526-531. https://doi.org/10.1007/BF02681976

Maripov, A. (1994). Slitless and lensless rainbow holography. Journal of Optics, 25(4), 131. https://doi.org/10.1088/0150-536X/25/4/001

Mukhopadhyay, A. K., & Mishra, D. (2024). Advances in experimental and numerical studies. Deformation and fracture in materials. CRC Press.

Mutaz, E., Serati, M., & Williams, D. J. (2024). Crack mode-changing stress level in porous rocks under polyaxial stress conditions. Acta Geotechnica, 19(2), 783-803. https://doi.org/10.1007/s11440-023-01994-2

Orazbayev, B., Kozhakhmetova, D., Orazbayeva, K., & Utenova, B. (2020). Approach to modeling and control of operational modes for chemical and engineering system based on various information. Applied Mathematics and Information Sciences, 14(4), 547-556. https://doi.org/10.18576/AMIS/140403

Panchenko, A., Voloshina, A., Milaeva, I., Panchenko, I., & Titova, O. (2018). The influence of the form error after rotor manufacturing on the output characteristics of an orbital hydraulic motor. International Journal of Engineering and Technology, 7(4), 1-5. https://doi.org/10.14419/ijet.v7i4.3.19542

Parsania, A., Kakavand, E., Hosseini, S. A., & Parsania, A. (2024). Estimation of multiple cracks interaction and its effect on stress intensity factors under mixed load by artificial neural networks. Theoretical and Applied Fracture Mechanics, 131, 104340. https://doi.org/10.1016/j.tafmec.2024.104340

Peng, T., He, F., Ren, D., Zhou, C., Xu, R., & Wang, C. (2024). Study on dynamic failure behavior of cracks in elliptical tunnel surrounding rock under dynamic load. Theoretical and Applied Fracture Mechanics, 133(Part A), 104541. https://doi.org/10.1016/j.tafmec.2024.104541

Salah, J. (2024). On uniformly starlike functions with respect to symmetrical points involving the Mittag-Leffler function and the Lambert series. Symmetry, 16(5), 580. https://doi.org/10.3390/sym16050580

Shan, Z., Zhao, L., Ni, W., Wu, J., Zhang, F., & Aliha, M. R. M. (2023). 3D numerical analysis of stability and onset of hydraulic fracture in the vertical-oblique-horizontal wells under wide range of in situ stresses. Fatigue & Fracture of Engineering Materials & Structures, 47(2), 413-438. https://doi.org/10.1111/ffe.14181

Sivadas, K., Natarajan, S., Parimi, C., Piska, R., & Hirshikesh (2024). Modeling dynamic crack growth in quasicrystals: unraveling the role of phonon-phason coupling. Engineering Fracture Mechanics, 304, 110140. https://doi.org/10.1016/j.engfracmech.2024.110140

Sunetchiieva, S., Yuan, P., Seresini, T., Pfeiffer, H., Wevers, M., & Glorieux, C. (2024). Early detection of fatigue-induced material changes by modulation of ultrasound in dynamically loaded structures. Structural Health Monitoring, 24(5), 2818-2836. https://doi.org/10.1177/14759217241266167

https://doi.org/10.24191/jmeche.v23i1.5703

Teixeira, R., Horas, C. S., De Jesus, A. M. P., Calçada, R., & Bittencourt, T. N. (2024). Innovative hierarchical fatigue analysis of critical riveted railway bridges: a case study. Engineering Structures, 317, 118629. https://doi.org/10.1016/j.engstruct.2024.118629

Wang, P., Fu, Y., Liu, C., Zhou, X., & Cai, M. (2024). Directional fracture patterns of excavated jointed rock mass within rough discrete fractures. Engineering Fracture Mechanics, 309, 110419. https://doi.org/10.1016/j.engfracmech.2024.110419

Wu, B., Chang, J., Wang, X., Shi, W., Li, C., & Chen, D. (2024). Research on the mechanism and application of high pre-tension on the crack-arresting effect of rockbolt anchorage. Buildings, 14(8), 2584. https://doi.org/10.3390/buildings14082584

Wu, G., Wang, W., & Peng, S. (2024). Analytical solution of the stress field and plastic zone at the tip of a closed crack. Frontiers in Earth Science, 12, 1370672. https://doi.org/10.3389/feart.2024.1370672

Xie, J., & Linder, C. (2024). Analysis of flexoelectric solids with a cylindrical cavity. Journal of Applied Mechanics, 91(1), 011007. https://doi.org/10.1115/1.4063145

Zeighami, V., Jafari, M., & Altenbach, H. (2024). A general analytical approach to the thermoelastic analysis of asymmetric anisotropic nanoplate with polygonal holes. Continuum Mechanics and Thermodynamics, 36(6), 1455–1480. https://doi.org/10.1007/s00161-024-01309-0

Zhao, R., Tao, M., Wang, S., Tao, T., & Wu, C. (2024). Mechanical response and failure mechanism of circular inclusion embedded in brittle materials under dynamic impact. International Journal of Impact Engineering, 194, 105088. https://doi.org/10.1016/j.ijimpeng.2024.105088

Zhou, T., Zhang, Y., Fan, Y., Chen, J., Zhou, C., Xie, H., & Zhu, J. (2024). Effect of high-temperature and strain rate on the mechanical and cracking behaviors of flawed sandstone under dynamic impact loading. Theoretical and Applied Fracture Mechanics, 131, 104405. https://doi.org/10.1016/j.tafmec.2024.104405

Zona, R., & Minutolo, V. (2024). A dislocation-based finite element method for plastic collapse assessment in solid mechanics. Archive of Applied Mechanics, 94(6), 1531-1552. https://doi.org/10.1007/s00419-024-02594-6

https://doi.org/10.24191/jmeche.v23i1.5703